Digital Elevation Model Fusion Using Spectral Methods

Evangelos G. Karakasis, Loukas Bampis, Angelos Amanatiadis, Antonios Gasteratos, Philippos Tsalides
School of Engineering, Democritus University of Thrace, Greece
ekarakas@pme.duth.gr, loukbabi@ee.duth.gr, aamanat@ee.duth.gr, agaster@pme.duth.gr, tsalides@ee.duth.gr

Abstract—This paper presents the application of different spectral methods, like Fourier series and polynomial-based expansions, to Digital Elevation Models (DEMs) in order to fuse their content. Two different fusion techniques: 1) a filter-based one and 2) a weighted average of expansion coefficients, are examined. Their performance is evaluated by using both ground-truth lidar data as well as fusion quality measures. The results point out that polynomial-based spectral expansions perform better than the traditional Fourier approach.

I. Introduction

Acquiring and utilizing high quality Digital Elevation Model (DEM) data is very critical for various types of commercial and scientific applications such as environmental monitoring, topographic analysis and mapping, communication modeling and remote sensing. Multiple sensor technologies have been developed and used for generating these models, including aerial stereo photography, airborne laser scanning and radar interferometry. However, depending on the selected type of sensor and technology used, various and different types of errors are introduced to the extracted DEM [1]. Other challenging issues of DEM post processing include grid spacing and interpolation methodologies [2], [3].

Despite their importance very limited open source models are available offering global coverage. Two of the most widely used models are the SRTM which offers $1''$ and $3''$ resolution for the USA and rest regions, respectively, and the ASTER GDEM which offers a 30m global resolution [4]. Due to the different providers of the aforementioned DEMs, their resolution, accuracy, and error characteristics vary a lot, making a challenging task the usage of both models for better and more efficient model representation.

By applying DEM fusion, their accuracy and resolution can be significantly improved along with their homogeneity and completeness [5]. Several methods have been proposed in the literature in order to perform such a fusion between ASTER and SRTM DEMs. In [6], the developed method applies a histogram shifting to the average elevation of the SRTM DEM, co-registering the relative ASTER DEM to the SRTM coordinates and filling the voids in the DEMs by an erosion technique from surrounding pixels. Two fusion methods are presented in [7], where the appropriate fusion weights are determined from sparse representations of local DEM patches, by minimizing their deviations assuming that are represented in a same sparse combination. A fusion method by considering

DEM quality through a weighted sum is proposed also in [8]. The produced model presents a geomorphological enhancement by generating trend surfaces as low frequency functions.

In this paper, two fusion strategies are presented, utilizing several spectral methods for acquiring improved DEM data. Traditionally, the most widely used spectral method is the Fourier expansion. However, several polynomial-based spectral expansions can also be successfully applied [9]. The proposed fusion strategies and the examined spectral methods are evaluated through a ground truth Lidar dataset and a comparative analysis is carried out in terms of DEM quality and consistency.

II. Spectral Methods

This section presents some basic theory on the computation of spectral methods, such as the discrete Fourier and Cosine Transform (DFT, DCT, respectively) [10] as well as Chebychev (CheT) [11] of first kind, Tchebichef (TchT) [12] and Legendre (LegT) [13] polynomial-based spectral expansions. The Chebyshev and Legendre are polynomials of continuous variable, while the Tchebichef is a polynomial family of discrete variable. It should also be noted that no classification between spectral and pseudo-spectral method takes place in this work.

Any $N \times M$ sized 2D digital signal (e.g. a DEM or an image), which may be perceived as a piecewise continuous function $f(t, k)$ of finite energy, can be approximately expanded as

$$f(t, k) \approx \sum_{n=0}^{N-1} \sum_{m=0}^{M-1} Kernel_{nm}^*(y_t, x_k) \cdot C_{nm} \qquad (1)$$

where $n \in [0, N-1] \subset \mathbb{Z}$, $m \in [0, M-1] \subset \mathbb{Z}$ and $\{C_{nm}\}$ are the expansion coefficients given by

$$C_{nm} = W_n W_m \sum_{k=0}^{N-1} \sum_{t=0}^{M-1} Kernel_{nm}(y_t, x_k) \cdot f(t, k) \quad (2)$$

$Kernel_{nm}(y_t, x_k)$ is formed using separable basis functions, while the star symbol (*) in Eq. (1) denotes complex conjugation. W_n and W_m are weighting factors, which depend on both the used kernel function and the orders (n, m). As basis function can be used any finite orthogonal set $\{\phi_n(x) \,|\, x \in [\alpha, \beta] \subset \mathbb{R}, \, n \in \mathbb{Z}\}$ such that

$$Kernel_{nm}(y_t, x_k) = \phi_m(y_t)\phi_n(x_k) \qquad (3)$$

It should also be noted that Eqs. (2) and (1) constitute the forward and inverse spectral transform, respectively.

A. Kernel Functions

Taking into account Eq. (3) and supposing that N and M are the 2D signal dimensions, the mathematical background required to calculate the basis set $\{\phi_n(x_k)\}$ is presented. Similarly, by replacing k, x, n and N with t, y, m and M, respectively, the set $\{\phi_m(y_t)\}$ can be calculated.

1) Fourier:

$$\phi_n(x_k) = e^{-inx_k} \ , \ \ x_k \in [0, 2\pi]$$

and

$$W_n = \frac{1}{N} \ , \ \ x_k = \frac{2\pi k}{N} \ , \ \ k = 0, 1, ..., N-1$$

2) Cosine:

$$\phi_n(x_k) = \omega_n \cdot cos(nx_k) \ , \ \ x_k \in [0, \pi]$$

where

$$\omega_n = \begin{cases} \frac{1}{\sqrt{N}}, & n = 0 \\ \sqrt{\frac{2}{N}}, & 1 \leq n < N \end{cases}$$

and

$$W_n = 1 \ , \ \ x_k = \frac{\pi(k + \frac{1}{2})}{N} \ , \ \ k, n = 0, 1, ..., N-1$$

3) Tchebichef:

$$\phi_n(x_k) = P_n(x_k) \ , \ \ x_k \in [0, N-1]$$

where

$$P_n(x) = A_1 P_n(x-1) + A_2 P_n(x-2)$$

and

$$A_1 = \frac{-n(n+1) - (2x-1)(x-N-1) - x}{x(N-x)}$$

$$A_2 = \frac{(x-1)(x-N-1)}{x(N-x)}$$

$$P_n(0) = \frac{(1-N)_n}{\beta(n,N)} \ , \ \ P_n(1) = P_n(0)\left(1 + \frac{n(n+1)}{1-N}\right)$$

$(a)_k$ is the Pochhammer symbol given by

$$(a)_k = a \cdot (a+1) \cdot ... \cdot (a+k-1)$$

and

$$\beta(n,N) = \sqrt{\rho(n,N)}$$

$$\rho(n,N) = \frac{N \cdot (N^2 - 1) \cdot (N^2 - 2^2) \cdot ... \cdot (N^2 - n^2)}{2n+1}$$

$$W_n = 1 \ , \ \ x_k = k \ , \ \ k, n = 0, 1, ..., N-1$$

4) Chebyshev:

$$\phi_n(x_k) = P_n(x_k) \ , \ \ x_k \in [-1, 1]$$

where

$$P_{n+1}(x) = 2xP_n(x) - P_{n-1}(x)$$

and

$$W_n = \begin{cases} \frac{1}{N} & n = 0 \\ \frac{2}{N} & 1 \leq n < N \end{cases} \ , \ \ x_k = cos(\pi\frac{k + \frac{1}{2}}{N})$$

$$k, n = 0, 1, ..., N-1$$

5) Legendre:
For the case of Legendre spectral expansion, the $\phi_n(x_k)$ which is used in the forward transform is given by

$$\phi_n(x_k) = \frac{2n+1}{2n+2}\left[\begin{array}{c} (u_k P_n(u_k) - P_{n-1}(u_k)) \\ (\hat{u}_k P_n(\hat{u}_k) - P_{n-1}(\hat{u}_k)) \end{array} \ - \ \right]$$

while for the inverse transform, $\phi_n(x_k)$ equals to

$$\phi_n(x_k) = P_n(x_k)$$

where

$$u_k = x_k + \frac{1}{N} \ , \ \ \hat{u}_k = x_k - \frac{1}{N}$$

$$x_k \in (-1, 1) \ , \ \ \hat{u}_k \in [-1, 1) \ , \ \ u_k \in (-1, 1]$$

$$P_{n+1}(x) = \frac{2n+1}{n+1}xP_n(x) - \frac{n}{n+1}P_{n-1}(x)$$

$$P_0(x) = 1 \ , \ \ P_1(x) = x$$

and

$$W_n = 1 \ , \ \ x_k = \frac{2k+1}{N} - 1 \ , \ \ k, n = 0, 1, ..., N-1$$

III. FUSION PROCESS

This section presents the process followed to fuse two DEMs. It is supposed that the DEMs are registered and no void areas occur.

Step 1 - Preprocessing: In the case where the used DEMs are characterized by different resolution, then the DEM with the lower one must be interpolated. In this work the cubic interpolation is adopted, nevertheless, other methods could also be used [14]–[16].

Step 2 - Forward Transform: The second step is to apply the forward transform of a spectral expansion method, like the ones described in section II, to the DEMs. This process projects the content of DEMs onto an orthogonal basis transforming the spatial information to a set of spectral/frequency coefficients $\{C_{nm}\}$.
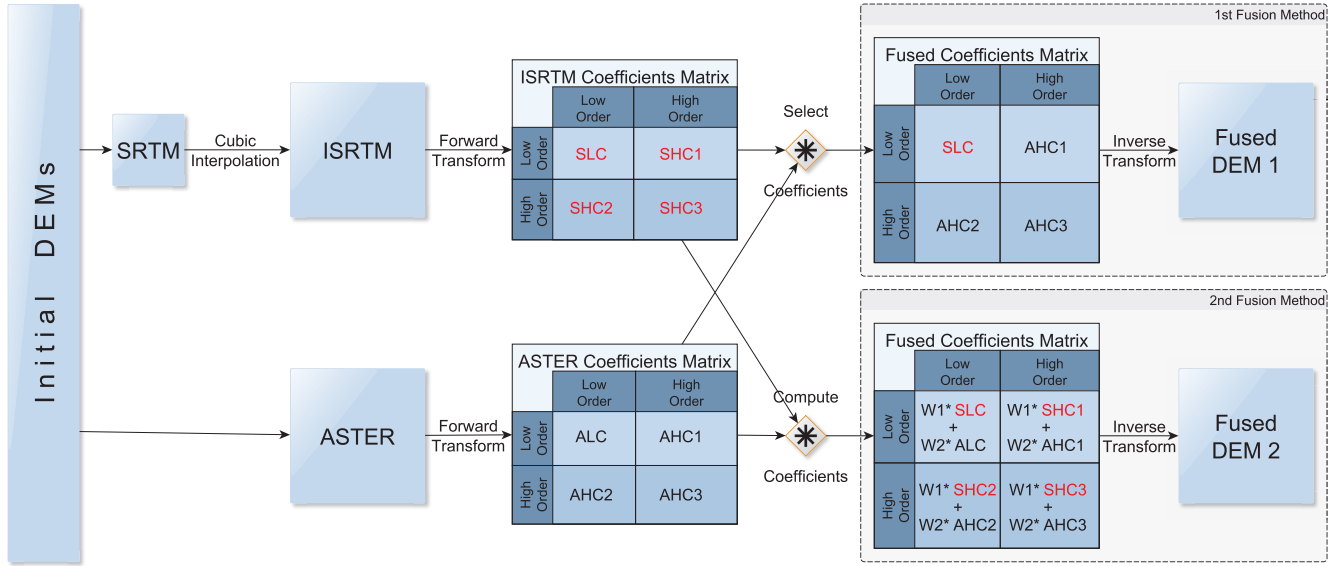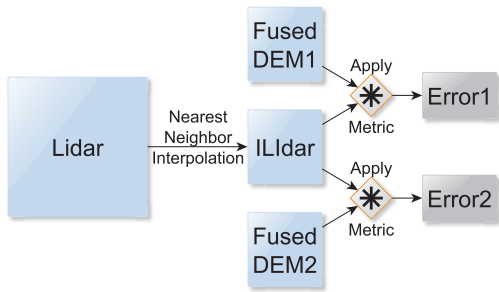
Fig. 1. Fusion process.

Fig. 2. Error measurement process between the DEMs resulted from the two fusion methods and the lidar data.

Step 3 - Fused Coefficients: In this step, the expansion coefficients of all the used DEMs ($\{C_{nm}^i\}$, $i = 1, 2, ..., k$, k: the number of different DEMs) are processed in order to form a new coefficient set, $\{\overline{C}_{nm}\}$. Two different methods of coefficients fusion are considered:

1) In the first one, each coefficient set subject to some filtering method. The main idea is to merge coarse and fine terrain features from different DEM sources. Since DEMs are 2D signals, four different coefficient thresholds, t_{11}, t_{12}, t_{21} and t_{22}, must be used in order to define low, high or band pass filters for both dimensions. Supposing that $\vec{t} = [t_{11}\ t_{12}\ t_{21}\ t_{22}]$ is the vector of thresholds and $F(C_{nm}^i, \vec{t})$ is a filtering operator representing all the aforementioned filter types, then, when k DEMs are used, the fused coefficients set can be calculated by

$$\overline{C}_{nm} = \sum_{i=1}^{k} F(C_{nm}^i, \vec{t})$$

For the case of two different DEMs as well as for $t_{11} =$

t_{12} and $t_{21} = t_{22}$ (which implies than only low and high-pass filters can be defined), the fusion process is illustrated in the "1st Fusion Method" of Fig. (1).

2) In the second fusion method, no filtering process takes place, instead, a weighted average of coefficients expansion is used. Weighting factors, w_i where $\sum_{i=1}^{k} w_i = 1$, applied to the corresponding $\{C_{nm}\}$ sets, lead to the new fused set $\{\overline{C}_{nm}\}$ according to the following equation:

$$\overline{C}_{nm} = \sum_{i=1}^{k} w_i C_{nm}^i$$

For the case of two different DEMs, the "2nd Fusion Method" is illustrated in the Fig. (1).

Step 4 - Inverse Transform: The final step, in order to fuse two or more DEMs, is to apply the inverse spectral transform to the fused coefficient set $\{\overline{C}_{nm}\}$ in order to return to spatial domain.

IV. EXPERIMENTAL STUDY

In this section, a performance comparative analysis of different spectral methods is presented. Two DEMs (SRTM [17], [18] - *Resolution (RES): 90m, Absolute Vertical Accuracy (AVA): 16m* - & ASTER [19] - *RES: 30m, AVA: 20m*) are used as inputs into the formerly presented fusion methodology. The studied geographic area (*Longitude range:* $2^o24'00.0"W$ *to* $2^o25'48.0"W$ *and Latitude range:* $43^o18'00.0"N$ *to* $43^o19'48.0"N$) has been selected due to the availability of lidar DEM [20] data with 1m resolution. These data are used as ground-truth in order to calculate the Mean Absolute Error (MAE) of the fused as well as initial DEMs (see Tables (I) and (II)).

TABLE I					

1ST FUSION METHOD: MEAN ABSOLUTE ERROR OF FUSED DEMS AND INITIAL DEMS (*interpolated SRTM & original ASTER*) WITH RESPECT TO GROUND TRUTH LIDAR DEMS

Mean Absolute Error					
	Spectral Methods				
$p_k^i = p_\ell^i$	Chebyshev	Legendre	Tchebichef	Fourier	Cosine
0.01	6.02	5.99	6.02	6.02	6.02
0.02	5.84	5.82	5.85	6.02	5.84
0.03	5.73	5.69	5.72	6.03	5.73
0.04	5.69	*5.61*	**5.64**	6.03	5.69
0.05	5.82	5.83	5.86	5.88	5.82
0.06	5.72	5.99	6.02	5.88	5.72
0.07	**5.66**	5.99	6.02	**5.85**	**5.66**
0.08	5.87	6.03	6.07	5.87	5.87
0.09	6.22	6.09	6.13	5.87	6.22
0.10	6.11	6.17	6.21	5.87	6.11
0.15	6.26	6.28	6.35	5.94	6.26
0.20	6.20	6.34	6.39	6.22	6.20
0.25	6.28	6.33	6.36	6.25	6.28
0.30	6.28	6.25	6.29	6.31	6.28
0.35	6.29	6.25	6.30	6.34	6.29
0.40	6.24	6.25	6.29	6.32	6.24
0.45	6.15	6.21	6.24	6.32	6.15
0.50	6.15	6.16	6.21	6.33	6.15
Initial DEMs					
$\overline{\text{SRTM}}$	5.94				
$\overline{\text{ASTER}}$	6.02				

TABLE II					

2ND FUSION METHOD: MEAN ABSOLUTE ERROR OF FUSED DEMS AND INITIAL DEMS (*interpolated SRTM & original ASTER*) WITH RESPECT TO GROUND TRUTH LIDAR DEMS

Mean Absolute Error					
	Spectral Methods				
W_1	Chebyshev	Legendre	Tchebichef	Fourier	Cosine
0.05	5.86	5.83	5.86	5.85	5.86
0.10	5.71	5.69	5.71	5.70	5.71
0.15	5.57	5.57	5.57	5.57	5.57
0.20	5.46	5.46	5.46	5.46	5.46
0.25	5.37	5.37	5.37	5.36	5.37
0.30	5.29	5.30	5.29	5.29	5.29
0.35	5.24	5.25	5.24	5.24	5.24
0.40	5.20	5.22	5.20	5.20	5.20
0.45	5.18	5.20	5.18	5.18	5.18
0.50	**5.17**	**5.20**	**5.17**	**5.17**	**5.17**
0.55	5.19	5.21	5.19	5.18	5.19
0.60	5.21	5.24	5.21	5.21	5.21
0.65	5.25	5.29	5.25	5.25	5.25
0.70	5.31	5.35	5.31	5.31	5.31
0.75	5.38	5.42	5.38	5.38	5.38
0.80	5.47	5.50	5.47	5.47	5.47
0.85	5.57	5.60	5.57	5.57	5.57
0.90	5.68	5.71	5.68	5.68	5.68
0.95	5.80	5.83	5.80	5.80	5.80
Initial DEMs					
$\overline{\text{SRTM}}$	5.94				
$\overline{\text{ASTER}}$	6.02				

A. Protocol

Since the used DEMs, SRTM, ASTER and the lidar data are characterized by different resolution, two interpolation processes should be conducted. Thus, a cubic and a nearest neighbor interpolation [15], [21] take place in order to properly scale the SRTM and lidar DEM, respectively.

1) 1st Fusion Method: As has already been mentioned two different fusion methods are studied. In the first one, the low-pass filter of Eq. (4) is applied on SRTM data, while the high-pass of Eq. (5) is applied on ASTER DEM.

$$LF(C_{nm}^1, k, \ell) = \begin{cases} C_{nm}^1 & \begin{aligned} 0 &\leq n \leq k \\ 0 &\leq m \leq \ell \end{aligned} \\ 0 & otherwise \end{cases} \quad (4)$$

$$HF(C_{nm}^2, k, \ell) = \begin{cases} 0 & otherwise \\ C_{nm}^2 & \begin{aligned} 0 &\leq n \leq N-1 \\ \ell &\leq m \leq N-1 \end{aligned} \\ C_{nm}^2 & \begin{aligned} k &\leq n \leq N-1 \\ 0 &\leq m \leq N-1 \end{aligned} \end{cases} \quad (5)$$

C_{nm}^i, where $i = 1, 2$ (1: SRTM & 2: ASTER), is the $(n+m)$-th order spectral coefficient, k and ℓ are the threshold values, while N and M are the signal dimensions. The fused coefficients are calculated as

$$\overline{C}_{nm} = LF(C_{nm}^1, k, \ell) + HF(C_{nm}^2, k, \ell) \quad (6)$$

By applying the inverse transform to the set $\{\overline{C}_{nm}\}$, the fused DEM, using the $1st$ fusion method, is produced.

In order to have a qualitative assessment of how close or far from zero value the thresholds k and ℓ are, we set

$$p_k^i = \frac{k}{N-1} \ , \ p_\ell^i = \frac{\ell}{M-1}$$

Since $k \in [0, N-1]$ and $\ell \in [0, M-1]$, then $p_k^i, p_\ell^i \in [0, 1]$. By attributing such values to k and ℓ, so as $p_k^i = p_\ell^i = \{0.01, 0.02, ..., 0.1, 0.15, ..., 0.5\}$, and measuring the Mean Absolute Error (MAE) between the fused and the ground-truth DEM, the corresponding results are presented in Table (I). The above process is graphically illustrated in Figs. (1) and (2)

2) 2nd Fusion Method: In the second fusion method a weighted average of expansion coefficients is used in order to create the fused DEM. The fused coefficients are calculated using Eq. (7).

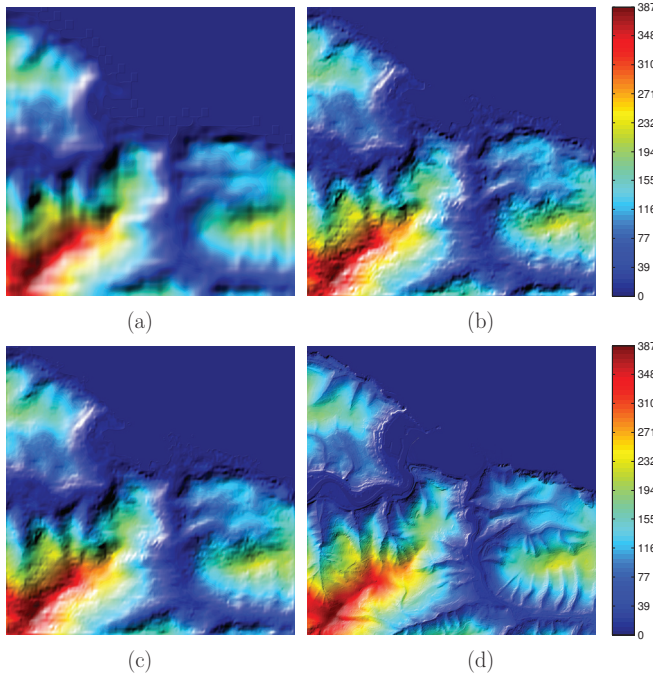$$\overline{C}_{nm} = w_1 C_{nm}^1 + w_2 C_{nm}^2 \quad (7)$$

Fig. 3. DEMs illustration for quality assessment of their resolution: (1) SRTM, (2) ASTER, (3) Fused, (4) Lidar. (*The colorbar scale is in meters.*)

Fig. 4. Square Error between the best fused DEMs and lidar data: (1) $1st$ fusion method, (2) $2nd$ fusion method. (*The colorbar scale is in meters.*)

(3) and (4) present shaded relief DEMs and error plots.

TABLE III
QUALITY MEASURES FOR THE BEST FUSION SETUPS.

Quality Measures	Fusion Method	Spectral Methods				
		Chebyshev	Legendre	Tchebichef	Fourier	Cosine
Q	1st	0.647	0.660	0.674	0.591	0.647
	2nd	**0.723**	0.706	**0.723**	0.621	**0.723**
Q_w	1st	0.659	0.648	0.651	0.622	0.659
	2nd	**0.724**	0.719	**0.724**	0.659	**0.724**
Q_e	1st	0.674	0.677	0.678	0.632	0.674
	2nd	**0.757**	0.753	**0.757**	0.692	**0.757**
MI	1st	0.574	0.581	0.589	0.590	0.574
	2nd	**0.607**	0.603	**0.607**	0.599	**0.607**

w_1 and w_2 are the weighting factors of the SRTM and ASTER expansion coefficients, respectively, for which it holds that $w_1 + w_2 = 1$. By applying the inverse transform to the set $\{\overline{C}_{nm}\}$, the fused DEM, using the $2nd$ fusion method, is produced.

By attributing the values $\{0.05, 0.1, 0.15, ..., 0.95\}$ to the weight w_1 and taking into account that $w_2 = 1 - w_1$, the corresponding MAE results between the fused and the ground-truth DEM are presented in Table (II). The above process is graphically illustrated in Figs. (1) and (2).

3) Other Quality Measures: Except using MAE, as mentioned above, the Mutual Information [22], given by Eq. (8), is also used.

$$MI(s, a, f) = \frac{I(s, f) + I(a, f)}{H(s) + H(a)} \quad \in [0, 1] \qquad (8)$$

Where s, a and f are the SRTM, ASTER and fused DEMs, respectively. $I(s, f)$ is the mutual information between s and f, and $H(s)$ is the entropy of s. Furthermore, Piella's metrics $(Q, Q_w, Q_e(\alpha) \in [-1, 1])$ [23] are very useful for evaluating the fusion process. The first two fusion quality measures, Q and Q_w, are quite similar, with the second being a weighted version of the first one. Furthermore, the main difference of Q_e, is that it also takes into account edge information with the parameter $\alpha \in [0, 1]$ expressing the importance of that information. The closer the value of above measures to 1, the better the quality of the fused DEM. Table (III) presents the values of the quality measures for the best setup of the examined spectral methods.

Finally, for the qualitative assessment of the used DEMs as well as the spread of square error across the fused result, Figs.
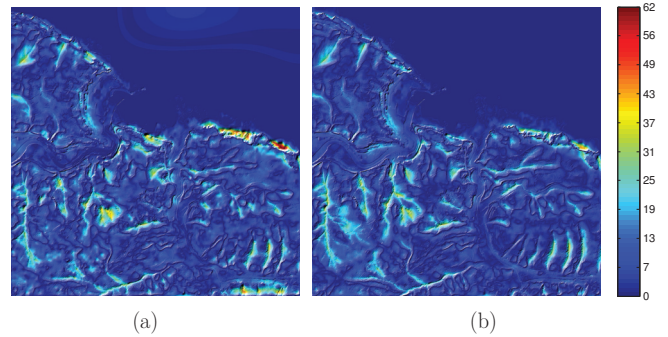
B. Results Evaluation

By examining Tables (I), (II) and (III) as well as Fig. (4), it can be directly concluded that the 2nd fusion method results in better fused output. The performance of the 2nd method owed to the fact that, unlike the 1st one, it combines all the spectral components from both DEMs. However, both methods lead to an output with improved vertical accuracy than the initial inputs.

Although the examined spectral methods present similar fusion performance in terms of MAE, an interesting result arises from Table (III). In this table, it can be seen that the Chebyshev, Tchebichef and Cosine expansions lead to better conveyance of edge and textural content to the fusion DEM, than the ones of Fourier and Legendre.

At this point, it should be noted that the Chebyshev and Cosine transforms results in identical behavior. This is expected, since the Chebyshev polynomial of first kind equals to $T_n(x_k) = cos(n \cdot arccos(x_k))$ and that, as stated in Section (II), $x_k = cos(\pi \frac{k+\frac{1}{2}}{N})$, then $T_n(x_k) = cos(n \cdot arccos(cos(\pi \frac{k+\frac{1}{2}}{N}))) = cos(n\pi \frac{k+\frac{1}{2}}{N})$ leading to the Cosine transform.

V. Conclusions

In this work five spectral methods are compared on the basis of DEM fusion and to the best of our knowledge, it is the first time that Chebyshev, exact Legendre, and Tchebichef expansions are used for such purpose. Additionally, two different fusion methods are considered: 1) filter-based and 2) weighted average, with the second to outperform the first one. Furthermore, a variety of measures, such as MAE based on lidar ground-truth as well as Mutual Information and Piella's metrics, has been used. Finally, a compact presentation of the forward and inverse transforms of the used spectral methods, is given. The success of the used spectral expansions triggers their investigation in more sophisticated fusion methodologies.

References

[1] P. F. Fisher and N. J. Tate, "Causes and consequences of error in digital elevation models," *Progress in Physical Geography*, vol. 30, no. 4, pp. 467–489, 2006.

[2] D. Maune, J. Maitra, and E. McKay, *Digital elevation model technologies and applications: the DEM users manual*. American Society for Photogrammetry and Remote Sensing, Bethesda, MD, 2001.

[3] A. Amanatiadis and I. Andreadis, "Performance evaluation techniques for image scaling algorithms," in *IEEE International Workshop on Imaging Systems and Techniques*, 2008, pp. 114–118.

[4] Y. S. Hayakawa, T. Oguchi, and Z. Lin, "Comparison of new and existing global digital elevation models: Aster g-dem and srtm-3," *Geophysical Research Letters*, vol. 35, no. 17, 2008.

[5] H. Papasaika, E. Kokiopoulou, E. Baltsavias, K. Schindler, and D. Kressner, "Fusion of digital elevation models using sparse representations," in *Photogrammetric Image Analysis*, 2011, pp. 171–184.

[6] M. Karkee, B. L. Steward, and S. A. Aziz, "Improving quality of public domain digital elevation models through data fusion," *Biosystems Engineering*, vol. 101, no. 3, pp. 293–305, 2008.

[7] K. Schindler, H. Papasaika-Hanusch, S. Schütz, and E. Baltsavias, "Improving wide-area dems through data fusion–chances and limits," in *Proceedings of the Photogrammetric Week*, vol. 11, 2011, pp. 159–170.

[8] T. Podobnikar, "Production of integrated digital terrain model from multiple datasets of different quality," *International Journal of Geographical Information Science*, vol. 19, no. 1, pp. 69–89, 2005.

[9] E. Karakasis, G. Papakostas, D. Koulouriotis, and V. Tourassis, "A unified methodology for computing accurate quaternion color moments and moment invariants," *IEEE Transactions on Image Processing*, vol. 23, no. 2, pp. 596–611, 2014.

[10] A. Jain, *Fundamentals of digital image processing*, ser. Prentice-Hall information and system sciences. Prentice Hall, 1989.

[11] Z. Omar, N. Mitianoudis, and T. Stathaki, "Two-dimensional chebyshev polynomials for image fusion," in *28th Picture Coding Symposium, PCS 2010*, 2010, pp. 426–429.

[12] R. Mukundan, S. Ong, and P. Lee, "Image analysis by tchebichef moments," *IEEE Transactions on Image Processing*, vol. 10, no. 9, pp. 1357–1364, 2001.

[13] K. Hosny, "Exact legendre moment computation for gray level images," *Pattern Recognition*, vol. 40, no. 12, pp. 3597–3605, 2007.

[14] A. Amanatiadis and I. Andreadis, "A survey on evaluation methods for image interpolation," *Measurement Science and Technology*, vol. 20, no. 10, p. 104015, 2009.

[15] I. Andreadis and A. Amanatiadis, "Digital image scaling," in *Proceedings of the IEEE Instrumentation and Measurement Technology Conference*, vol. 3, 2005, pp. 2028–2032.

[16] A. Amanatiadis, I. Andreadis, and K. Konstantinidis, "Fuzzy area-based image scaling," in *Proceedings of the IEEE Instrumentation and Measurement Technology Conference*, 2007, pp. 1–6.

[17] B. Rabus, M. Eineder, A. Roth, and R. Bamler, "The shuttle radar topography mission - a new class of digital elevation models acquired by spaceborne radar," *ISPRS Journal of Photogrammetry and Remote Sensing*, vol. 57, no. 4, pp. 241–262, 2003.

[18] T. Farr, P. Rosen, E. Caro, R. Crippen, R. Duren, S. Hensley, M. Kobrick, M. Paller, E. Rodriguez, L. Roth, D. Seal, S. Shaffer, J. Shimada, J. Umland, M. Werner, M. Oskin, D. Burbank, and D. Alsdorf, "The shuttle radar topography mission," *Reviews of Geophysics*, vol. 45, no. 2, 2007.

[19] H. Reuter, A. Nelson, P. Strobl, W. Mehl, and A. Jarvis, "A first assessment of aster gdem tiles for absolute accuracy, relative accuracy and terrain parameters," in *International Geoscience and Remote Sensing Symposium (IGARSS)*, vol. 5, 2009, pp. V240–V243.

[20] The lidar DEM data website. [Online]. Available: http://b5m.gipuzkoa.net/

[21] A. Amanatiadis, L. Bampis, and A. Gasteratos, "Accelerating image super-resolution regression by a hybrid implementation in mobile devices," in *IEEE International Conference on Consumer Electronics*, 2014, pp. 335–336.

[22] G. Qu, D. Zhang, and P. Yan, "Information measure for performance of image fusion," *Electronics Letters*, vol. 38, no. 7, pp. 313–315, 2002.

[23] G. Piella, "New quality measures for image fusion," in *Proceedings of the Seventh International Conference on Information Fusion, FUSION 2004*, vol. 1, 2004, pp. 542–546.